

In-situ

K C , W , L ,*, L H , C , L , L ,
W , K E , L L , G , T P J

Gemmological Institute, China University of Geosciences, Wuhan 430074, PR China
 Hubei Gem and Jewelry Engineering Technology Research Center, Wuhan 430074, PR China
 School of Materials Science and Engineering, Huazhong University of Science and Technology, Wuhan 430074, PR China
 Mechanical Engineering, University of Birmingham, Birmingham B15 2TT, UK
 School of Electrical and Electronic Engineering, Huazhong University of Science and Technology, Wuhan 430074, PR China
 WMG, Materials Engineering Centre, University of Warwick, CV4 7AL Coventry, UK

ARTICLE INFO

Keywords:

T
C
S
C
B

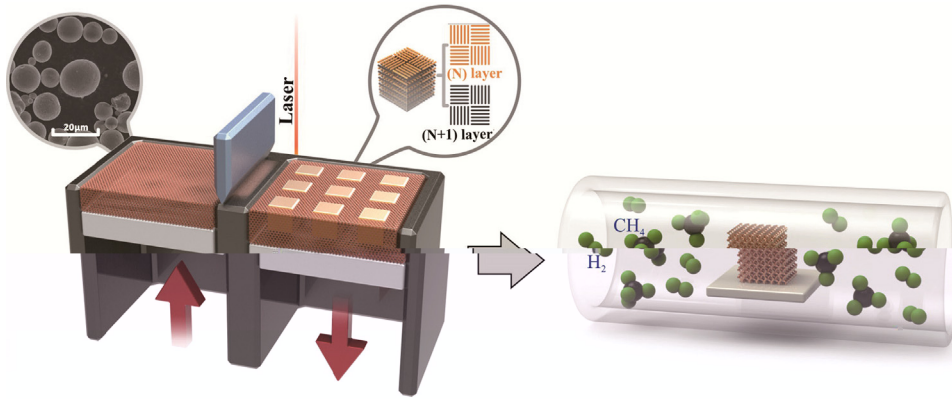
ABSTRACT

C , - (3DG) . H
 (SLM) (3D)
 . G in-situ (CVD) C
 SLM 3DG ff A CVD
 ff . T 3DG/ ff ()
 (EMI) 88% 27% SE 32.3 B EMI ffi-
 (SE) 47.8 B 2.7 GH 2-18 GH .
 T SLM

1. Introduction

G , sp^2
 (2630 2^{-1}) 1 ,
 ($2 \cdot 10^5 \cdot 2 \cdot V^{-1} \cdot -1$)
 ($6 \cdot 5000 \cdot W^{-1} \cdot K^{-1}$) 2 . H , $\pi-\pi$
 (2D)
 ff
 3 . A
 C
 (3DG)
 fi ($6 \cdot 0.6 \cdot -2$) 4
 (699.7%), fi
 (2DG), 4 , 5 , 6,7 ,
 (EMI) 8
 3DG
 9 , 10 ,
 . H . F
 ff
 13 . S
 ()
 14 . D
 15 . M
 CVD
 16 . B

*C : G I , C U G , W 430074, PR C .
 E-mail address: @ . (.L).



Copper substrate fabricated via SLM

Graphene growth on SLM copper via CVD

Fig. 1. Schematic diagram of the SLM process for copper substrate fabrication and subsequent CVD for graphene growth. The SLM process involves a laser scanning a copper powder bed on a substrate, building up layers (N and N+1). The CVD process involves placing the SLM-fabricated copper substrate in a tube furnace with CH₄ and H₂ gases.

3. Results and discussion

3.1. Formation of SLM copper

3.1.1. SLM manufacturing of copper under different line energy densities

The SLM process parameters include laser power (W) and scanning speed (mm/s). The line energy density (J/mm) is calculated as $\frac{\text{Laser Power}}{\text{Scanning Speed}}$. The process is optimized to achieve different microstructures: weak sintering, unstable melting, continuous track, and excessive melting.

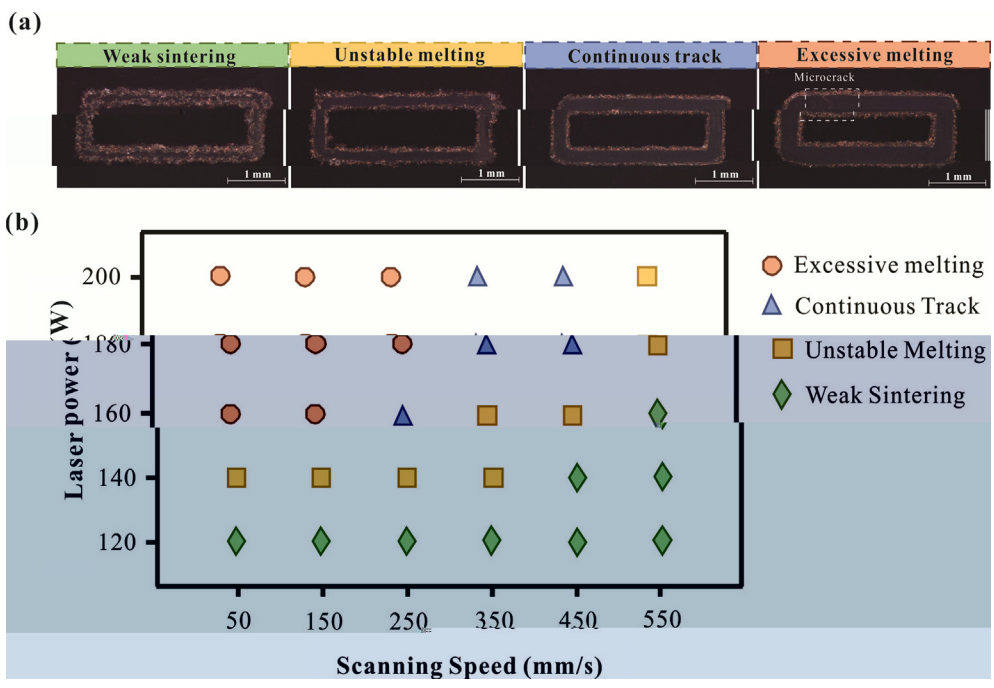


Fig. 2. SEM images of SLM copper tracks under different conditions: (a) Weak sintering, (b) Unstable melting, (c) Continuous track, and (d) Excessive melting. (b) is a scatter plot showing the relationship between Laser power (W) and Scanning Speed (mm/s) for the four conditions.

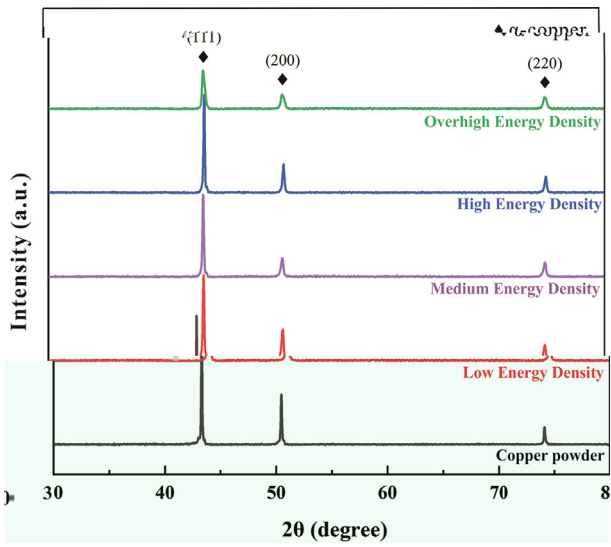


Fig. 3. RD

3.1.2. Formation of anisotropic microstructure under different volumetric energy density

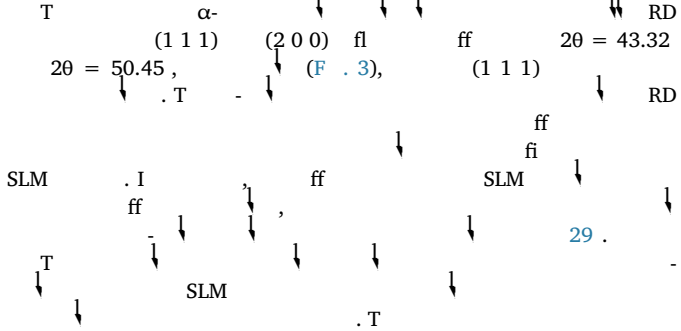


Fig. 4. O

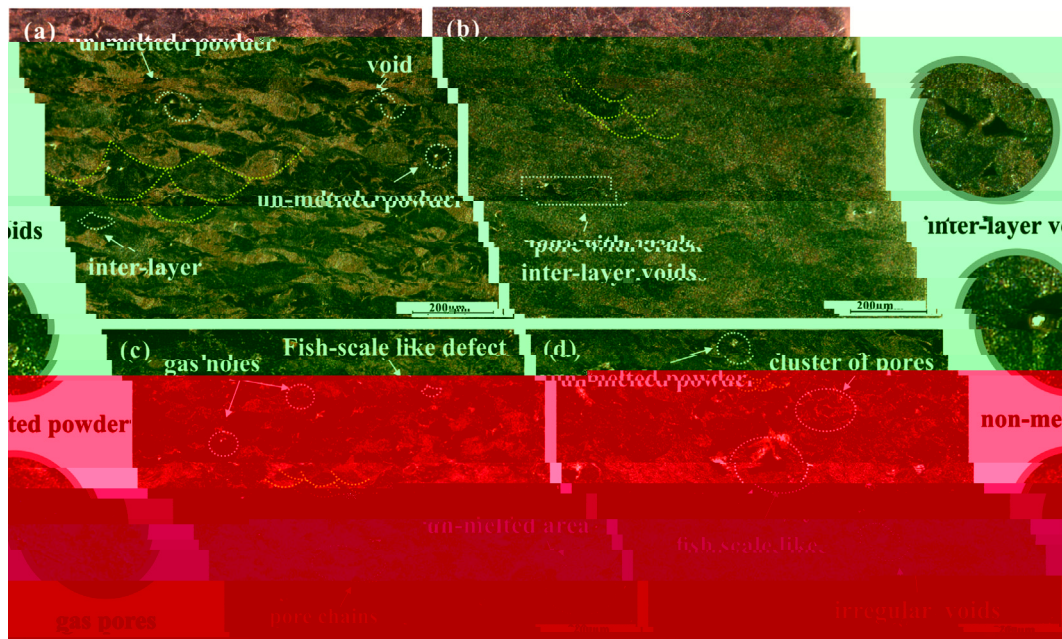


Fig. 4. O (285 J/cm³), (128 J/cm³), (3000 J/cm³), (857 J/cm³)

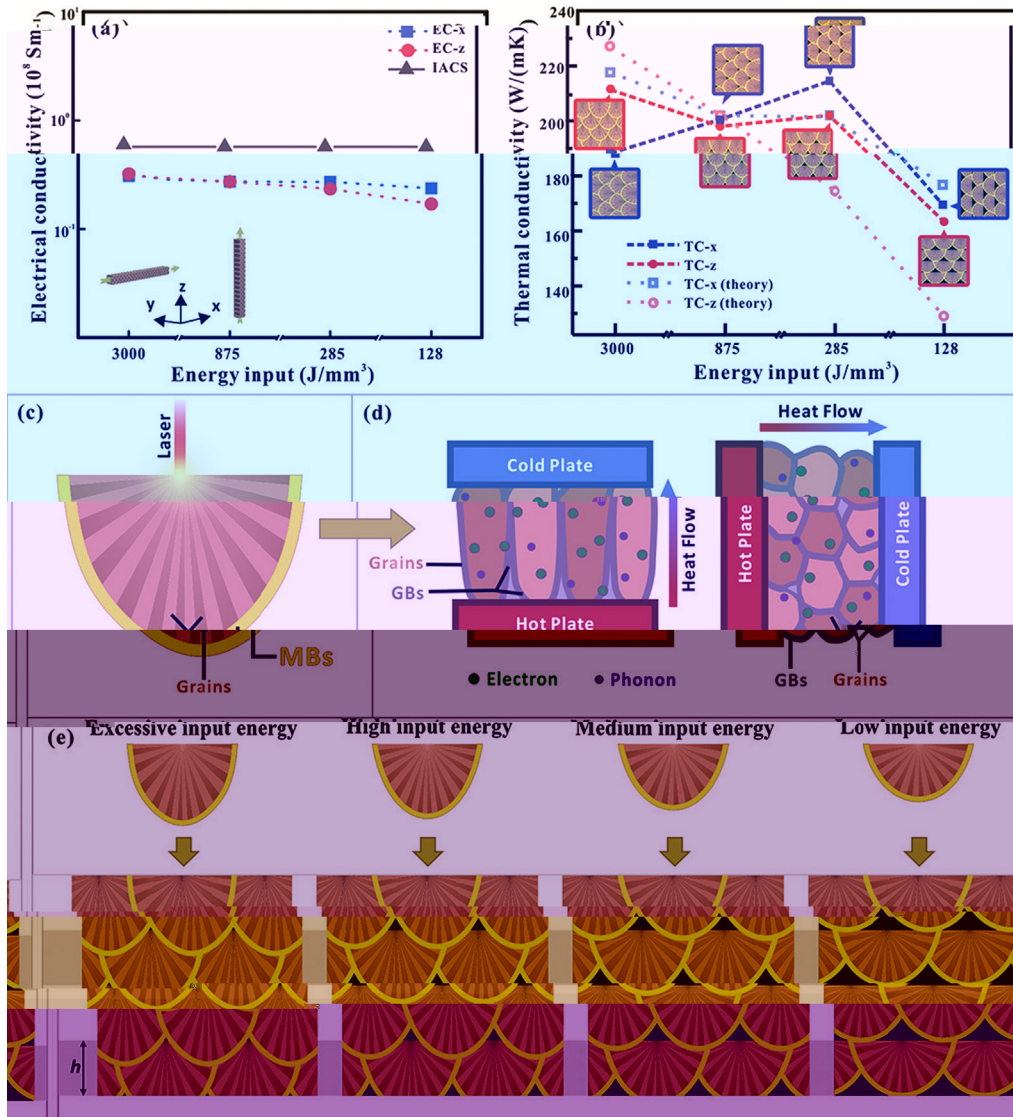


Fig. 7. (a) Electrical conductivity vs. energy input for EC-x, EC-z, and IACS. (b) Thermal conductivity vs. energy input for TC-x, TC-z, and their theoretical values. (c) Schematic of laser irradiation. (d) Schematic of heat flow through grains and grain boundaries (GBs) between hot and cold plates, showing electron and phonon transport. (e) Schematic showing the effect of excessive, high, medium, and low input energy on the material's microstructure.

3.3. Morphology and structure of CVD 3DG/Cu porous scaffolds

The morphology and structure of CVD 3DG/Cu porous scaffolds were investigated using SEM, TEM, and EDS. The scaffolds were prepared by *in-situ* CVD of Cu on 3DG. The SEM images (Fig. 8a, b) show the porous structure of the scaffolds, with a pore size of approximately 450 μm. The TEM images (Fig. 8c-d) show the atomic structure of the Cu nanowires, with a diameter of approximately 40 nm. The EDS analysis (Fig. 8e-g) shows the presence of Cu and C in the scaffolds. The Raman spectra (Fig. 8h) show the characteristic peaks of Cu and C, with a D/G ratio of approximately 0.15. The XRD patterns (Fig. 8i) show the characteristic peaks of Cu and C, with a peak intensity ratio of approximately 1:1. The mechanical properties of the scaffolds were investigated using compression tests, showing a compressive strength of approximately 1590 MPa and a compressive modulus of approximately 2699 GPa. The scaffolds were also investigated for their electrical and thermal properties, showing a high electrical conductivity and a low thermal conductivity.

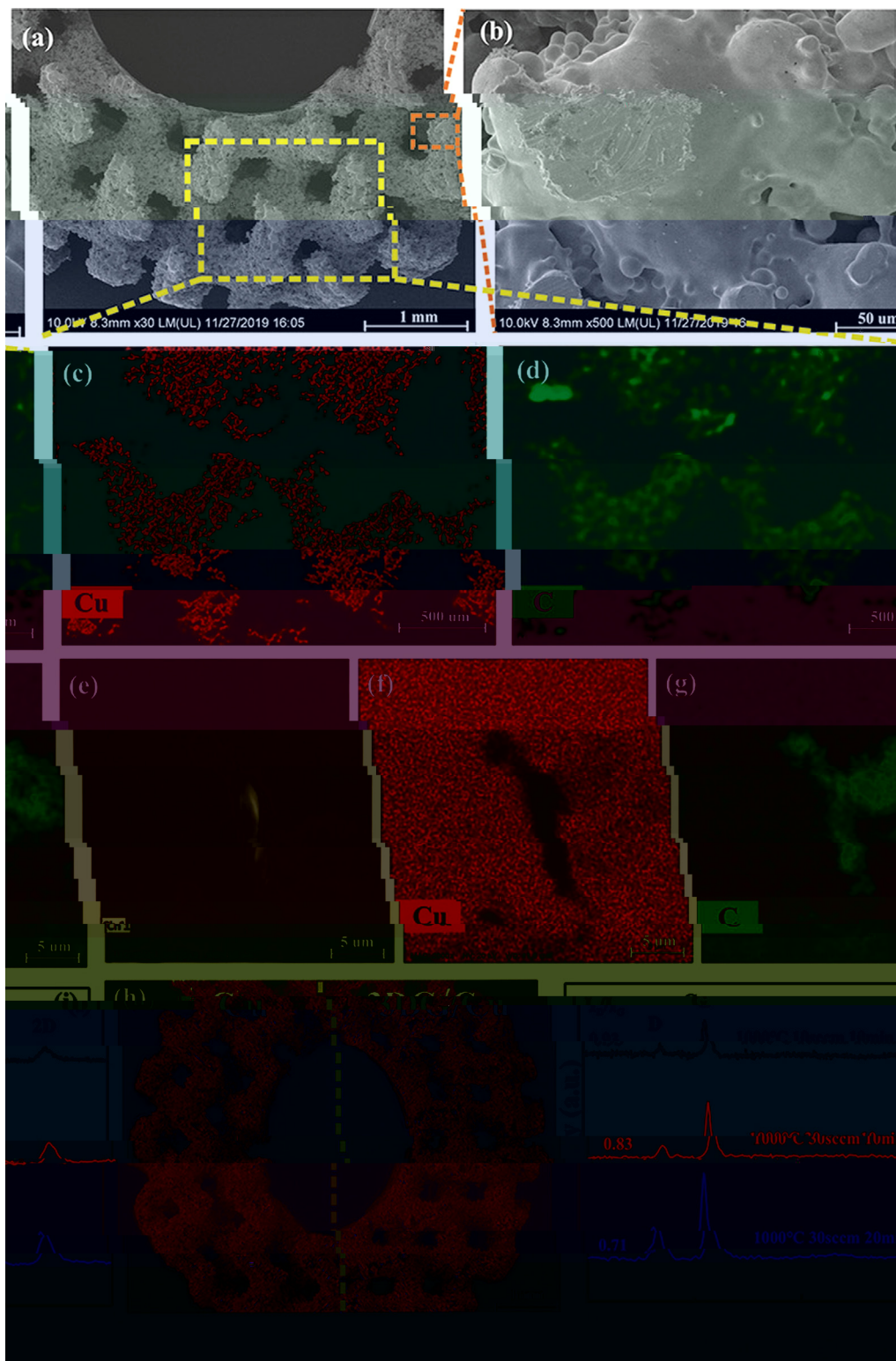


Fig. 8. (a) SEM image of 3DG/Cu porous scaffold at 1 mm scale. (b) SEM image of 3DG/Cu porous scaffold at 50 μm scale. (c) EDS map for Cu at 500 μm scale. (d) EDS map for C at 500 μm scale. (e) EDS map for Cu at 5 μm scale. (f) EDS map for C at 5 μm scale. (g) EDS map for C at 5 μm scale. (h) Raman spectra showing peaks at 0.71 and 0.83.

3.4. Thermal property and EMI shielding effectiveness of 3DG/Cu porous scaffolds

The thermal stability of 3DG/Cu porous scaffolds was evaluated by TGA. The TGA curves show that the weight loss of 3DG/Cu porous scaffolds is about 26.8% at 1000 °C, which is attributed to the decomposition of the 3DG scaffold. The EMI shielding effectiveness of 3DG/Cu porous scaffolds was evaluated by the reflection coefficient (R) and the absorption coefficient (A). The R and A values of 3DG/Cu porous scaffolds are 14.8% and 26.8%, respectively.

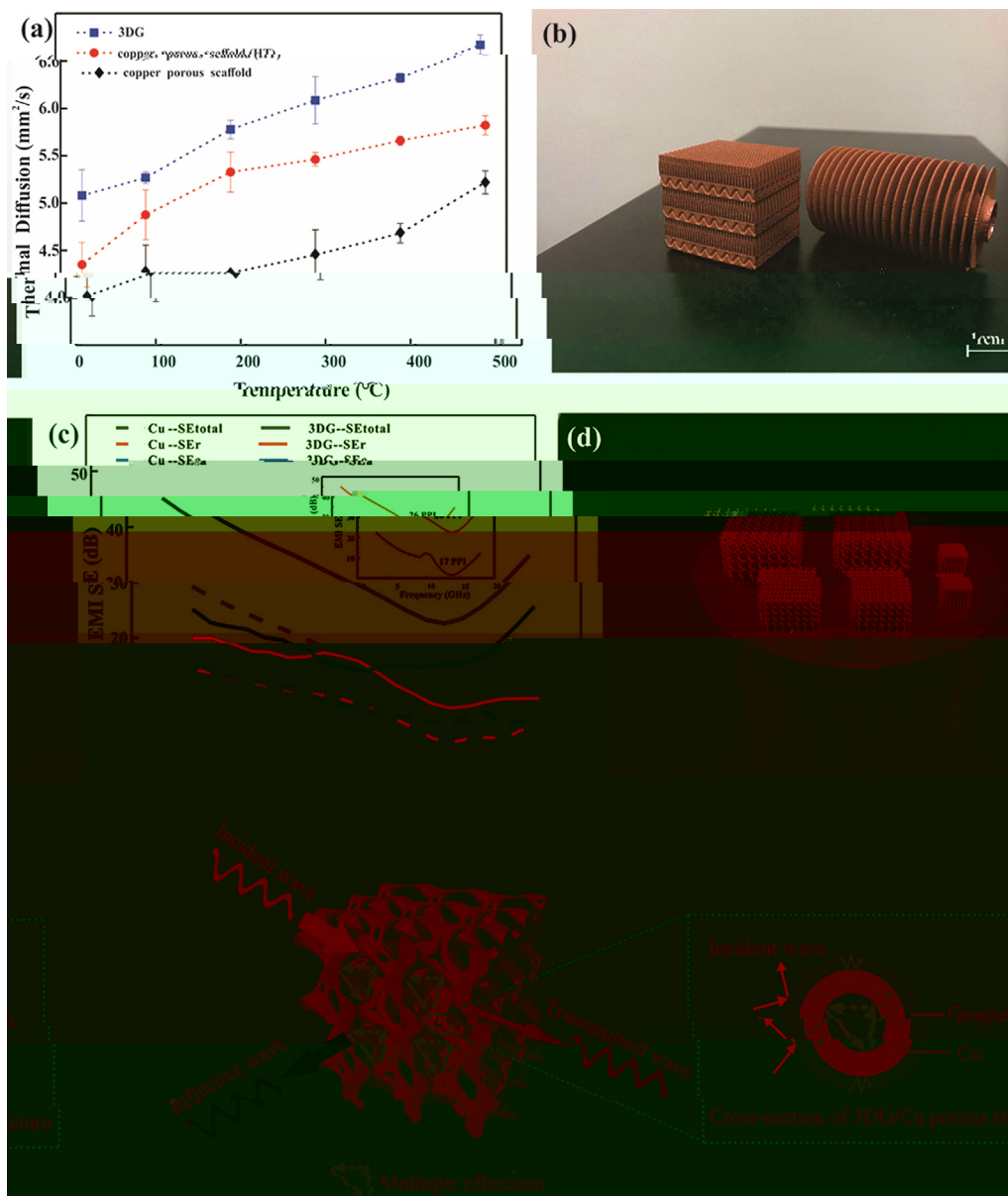


Fig. 9. P 3DG/C ff ; () ff ; () SLM ff ff () S 3DG/C fl EMI. (F)

Table 1

Coating materials	Substrate	Method	Maximum shielding efficiency (dB)	Improvement of thermal property (%)	Ref
G	G	I + + ↓ + ↓	37	-	50
G	PS	H - ↓ ↓ ↓	29.3	-	56
G	PMMA	S ↓ + ↓ +	19	-	57
C /G	/C	A ↓ S fi + ↓ ↓ ↓	-	8.5	58
G	N	F + CVD	-	554	59
G	C -N	H ↓ + ↓	20	-	60
G	C	P + CVD	-	2.4	61
G	C	F - + ↓ ↓	47	6.3	62
G	C	CVD + SLM	47.8	27	T

Note: ↓ (↓ ↓)-PPMA, ↓ -PS.

HT
in-situ (F . 9a). S
 3DG/C ff
 HT
 1-2 . I ,
 . W
 SLM fl
 (F . 9b),
 500 μ)
 . G
 (T ↓ 1). I
 N
 T
 EMI, EMI SE,
 (EM)
 2-18 GHz (F . 9c),
 . W *in-situ*
 SE
 ff
 47.8 B (88.2%)
 3DG/C
 . J K
 44
 EMI
 . T EMI SE
 133%
 R J K 45) 20 110 PPI ()
 EMI
 . W
 17 26 PPI (F . 9c insert) 105%
 EMI SE. I , EMI
 ff
 3DG/C 26 PPI
 32.3 B, 99.9%
 (30
 3DG/C T ↓ 1. I
 3D
 T
 (SE_a) fl EMI fl (SE_r),
 (EM) 47 ,
 48 . R, 49
 T
 50 . R EMI
 C 51 . F
 52 S O₂ 53 . W

SE_r SE_a
 fi
 F . 9e. W
 3DG/C ff
 fl
 3DG/C
 fi
 EM
 fi
 EM
 SE_r. O
 ff
 ff
 EM
 EM
 . T
 44 . T
 3D
 EM
 CVD
 . I
 R
 S 3.3
 EM
 55 . I
 . O
 3DG/C
 ff
 . T

4. Conclusions

A 3DG/C ff
in-situ CVD
 T ff
 . W
 3DG/C
 EMI SE
 15.9 (32.3 B,
 47.8 B (88.2%)), 26.8%
 ff . T 3DG/C
 fl
 . T J
 3DG/C
 EMI ff

Credit authorship contribution statement

Kaka Cheng: C , M , F ,
 W . Wei Xiong: V , I , W ,
 . Yan Li: W & , F ,
 R , S . Liang Hao: F . Chunze Yan:
 R , F . Zhaoqing Li: V . Zhufeng Liu:
 F ↓ . Yushen Wang: I , S . Khamis Essa:
 W - & . Li Lee: D . Xin Gong: S .
 Ton Peijs: W - & , S .

Declaration of Competing Interest

T ↓ fl

Acknowledgement

T ↓ N ↓ S ↓ F ↓ C ↓ (N . 51671091, N . 51902295, N . 51675496). T ↓ N ↓ J ↓ C ↓ U ↓ C ↓ (N . CUG170677) ↓ H ↓ P ↓ N ↓ S ↓ F ↓ (N . 2019 CFB264).

Appendix A. Supplementary data

S ↓ /10.1016/J . 2020.105904. //

References

1 B RG, N N, M K, M S. G : ↓ ↓
 2 B ↓ AA, G S, B W, C ↓ L, T ↓ D, M F, ↓ S
 3 L ↓ H, C M, P H, P O, S L ↓ G, ↓ I
 4 K M, K J, J B, C ↓ K, JH, A JH. G . ACS A ↓ M I 2016;8(36):24112–22.
 5 P ↓ C M, H M, T M, ↓ L D. P . ACS N 2017;11(8):7950–7.
 6 A C ↓ B 2020;262:118266–76.
 7 L ↓ J, W, C LL, J SH, W G, ↓ L ↓ C-G
 2017;101:50–8.
 8 HQ, L SW, C LH, J SH, H HQ. S ↓ J. M C A
 2018;6(42):21216–24.
 9 D ↓ TM, S P, D ↓ P, K ↓ J, K M, A T, ↓ 3D
 2017;1(4):467–70.
 10 Q L, L L. T ↓ RSC A 2014;4(72):38273–80.
 11 D ↓ H L SP, N, W JG. 3D
 M S₂ ↓ P A 2016;90:424–32.
 12 L L, ↓ W, S CO, H MK, HL, D W, ↓ S ↓ fl EM
 201803938. ↓ A F M 2018. // ↓ /10.1002/
 201803938.
 13 L J, P ↓ C, R G, ↓ N ↓ D, ↓ G . ACS N
 2013;7(7):6001–6.
 14 J SH, A S, G A. L ↓ ↓
 ↓ A C I E 2017;56:15520–38.
 15 I ↓ T ↓ S K, K M, T T, T ↓ K, ↓ T
 ↓ PCCP 2018;20(9):6024–33.
 16 S ↓ K, D N, M W, C, V N, E ↓ J. T ↓ ↓
 ↓ J B S 2002;149(8):370–7.
 17 C H, S M, S WH, L G, H Q, ↓ P ↓ 3D
 ↓ S 2011;7(22):3163–8.
 18 K H, G M, J ↓ I, H J, W C, C M. U
 ↓ M 2019;1(4):1077–87.
 19 S Q, F ↓ L W, L H, L ↓ C
 ↓ A M 2017;29(31):1701583–90.
 20 ↓ G C, L, T H, ↓ D, W ↓ T
 ↓ ACS N 2019. // ↓ /10.1021/
 21 C C, H ↓ B N, J, C S, L F, ↓ 3D T 6A 4V ↓
 ff ↓ M D 2019;175:107824–33.
 22 S š č J, B ž č D. T ff N B ↓ SLM. S C
 T ↓ 2016;307:407–17.

22 R DC, HB, L J, L SJ, J W, ↓ R, ↓ M ↓ M S E A-S
 T-N ↓ 2020;771:138586–95.
 23 L ↓ C W, A J, K S, N J, ↓ D, ↓ S ↓ 2009;324(5932):1312–4.
 24 C P, R WC, G LB, L BL, P SE, C HM. T ↓ fl ↓
 ↓ N M 2011;10:424–8.
 25 J SD, D ↓ S, G ↓ L, K JP, H ↓ JV, V ↓ K.
 I fl ↓ J M P T 2019;270:47–58.
 26 W, H L, L ↓ T D, C Q, F ↓ Eff ↓ ↓ ↓
 ↓ M D 2019;170:107697–708.
 27 G DD, M W, W ↓ K, P R. L ↓ I M R
 2013;57(3):133–64.
 28 L E, T S, C L, F A. Eff ↓ ↓ ↓ 316L (SLM)
 ↓ J M P T 2017;249:255–63.
 29 ↓ S, W ↓ L, J, W P, C ↓ T 6A 4V. A ↓ P A: M S
 P 2018;124:685–98.
 30 L ↓ M S, D W, S C. I ↓ M D
 2015;87:797–806.
 31 L CLA, M S, T M, A ↓ RC, W PJ, L PD. T ff
 2019;166:294–305.
 32 T ↓ K ↓ T WQ, T J, D M, M ↓ D, ↓ R ↓
 ↓ α/β T-6A-4V. S R 2016;6:26039–48.
 33 K H, T P, L NH, T SB, C CK. G ↓ T-6A-4V ↓ V
 P P 2016;11(3):183–91.
 34 R fi HK, K NV, G H, S TL, S BE, M ↓
 6 ↓ 4 J M E P 2013;22(12):3872–83.
 35 T ↓ K ↓ T J, V G, P Q, ↓ G, ↓ A ↓
 ↓ T-6A-4V. J A C 2015;646:303–9.
 36 R DA, M LE, M H ↓ ↓ N ↓
 ↓ W H. Eff ↓ A M 2011;59(10):4088–99.
 37 ↓ ↓ ↓ W H. Eff ↓ C-2.4N-0.7S ↓ J A C
 2018;743:258–61.
 38 K S. W ↓ S E 2003;23:309–48.
 39 L G ↓ G J ff R, G N P. E ↓ C (111). N
 L 2010;10(9):3512–6.
 40 L S, C WW, C ↓ L ↓ R ff R S. E ↓ N
 C ↓ N L 2009;9(12):4268–72.
 41 W, C, ↓ W H, SQ, ↓ L. A ↓ C
 2020;161:479–85.
 42 F AC, M JC, S V, C ↓ C, L M, M F, ↓ R
 ↓ P R L 2006;97(18):187401–4.
 43 S ↓ G ↓ J SH, F PC, H HQ. H ↓ ↓
 M L 2017;200:97–100.
 44 J K, H, J, C J, D ↓ F ↓ C-N ↓ CNT.
 A ↓ S S 2014;311:351–6.
 45 R J K, M DP, A ↓ C, M S, S ↓ MK. E ↓ EMI ↓
 ↓ C ↓ P A 2018;12:475–84.
 46 S ↓ B, L ↓ W, ↓ W. C ↓ (EMI) ↓ ACS
 A ↓ M I 2016;8(12):8050–7.
 47 L N, H ↓ D, F, H ↓ L ↓ G ↓ 00 0.59979 ↓ J(L 7T (A ↓)-340.55400 0.

53 M 2019;34(5):489–98.
W B, C M, L M. R . A M

54 C H, W S, J , J, C J, S ff F₃O₄
2014;26:3484–9.
2019;121:139–48.
W L, J, Q. T ff MWCNT
-MWCNT . J M S : M B

56 D , P GR, H P, Q F, M B , ML. Effi . J. M
2015;26(3):1895–9.

57 C 2012;22:18772–4.
HB, Q, WG, H , T . ACS A M I

58 S A, U N, T V. T
2011;3:918–24.
M R 2016. :// . /10.1051/ /2016021.

59 P MT, J H, R ff RS, S L. T . N L
2012;12:2959–64.

60 J K, H, H , D . P C -N M L
2017;122:244–7.

61 R H, L S, B S, K TW, L DS, L HJ, T
. S R 2015. :// . /10.1038/ 12710.
T, F SG, L , G Q, L G, R KP, S

62 . M S E A-S 2020. :// . /10.1016/J
.2019.105670.

63 R DA, M LE, M E, H DH, M JL, M BI, . A
N

64 M 2011;59(10):4088–99.
E SF, L KC, S VK, M IC. T . J T
E 1973;1(1):10–38.